A Clock Directly Linking Time to a Particle's Mass

Shau-Yu Lan *et al.*

Science **339**, 554 (2013);
DOI: 10.1126/science.1230767

interrelationships between diet, microbiota, and many facets of host physiology can be explored in detail in these "personalized" gnotobiotic mouse models. These models may be useful for developing new and more effective approaches for treatment and/or prevention. In addition, studies of other forms of malnutrition that take an approach analogous to that described here could also provide insights about the contribution of the gut microbiome to this global health problem.

References and Notes

1. United Nations (UN) Inter-Agency Group for Child Mortality Estimation, *Levels & Trends in Child Mortality Report* (2011); www.childinfo.org/files/Child_Mortality_Report_2011.pdf.
2. WHO Multicentre Growth Reference Study Group, *Acta Paediatr. Suppl.* **450**, 76 (2006).
3. WHO, UN Children's Fund, *WHO Child Growth Standards and the Identification of Severe Acute Malnutrition in Infants and Children* (2009); www.who.int/nutrition/publications/severemalnutrition/9789241598163/en/index.html.
4. C. D. Williams, B. M. Oxon, H. Lond, *Lancet* **226**, 1151 (1935).
5. T. Ahmed, S. Rahman, A. Cravioto, *Indian J. Med. Res.* **130**, 651 (2009).
6. C. Gopalan, in *Calorie Deficiencies and Protein Deficiencies: Kwashiorkor and Marasmus: Evolution and Distinguishing Features*, R. A. McCance, E. M. Widdowson, Eds. (Churchill, London, 1968), pp. 48–58.
7. M. H. Golden, *Lancet* **319**, 1261 (1982).
8. H. Ciliberto *et al.*, *BMJ* **330**, 1109 (2005).
9. C. A. Lin *et al.*, *J. Pediatr. Gastroenterol. Nutr.* **44**, 487 (2007).
10. T. Yatsunenko *et al.*, *Nature* **486**, 222 (2012).
11. R. E. Black *et al.*, *Lancet* **371**, 243 (2008).
12. WHO, World Food Programme, UN System Standing Committee on Nutrition, UN Children's Fund, *Community-Based Management of Severe Acute Malnutrition* (2007); www.who.int/nutrition/topics/statement_commbased_malnutrition/en/index.html.
13. Materials and methods are available as supplementary materials on *Science* Online.
14. L. Lagrone, S. Cole, A. Schondelmeyer, K. Maleta, M. J. Manary, *Ann. Trop. Paediatr.* **30**, 103 (2010).
15. J. Liu *et al.*, *J. Clin. Microbiol.* **50**, 98 (2012).
16. M. Taniuchi *et al.*, *Diagn. Microbiol. Infect. Dis.* **71**, 386 (2011).
17. M. Taniuchi *et al.*, *Am. J. Trop. Med. Hyg.* **84**, 332 (2011).
18. M. Taniuchi *et al.*, *Diagn. Microbiol. Infect. Dis.* **73**, 121 (2012).
19. S. Devkota *et al.*, *Nature* **487**, 104 (2012).
20. N. Crum-Cianflone, *Am. J. Med. Sci.* **337**, 480 (2009).
21. T. Itoh, Y. Fujimoto, Y. Kawai, T. Toba, T. Saito, *Lett. Appl. Microbiol.* **21**, 137 (1995).
22. M. F. Fernández, S. Boris, C. Barbés, *J. Appl. Microbiol.* **94**, 449 (2003).
23. Y. Kato-Mori *et al.*, *J. Med. Food* **13**, 1460 (2010).
24. A. A. Salyers, S. E. West, J. R. Vercellotti, T. D. Wilkins, *Appl. Environ. Microbiol.* **34**, 529 (1977).
25. H. Sokol *et al.*, *Proc. Natl. Acad. Sci. U.S.A.* **105**, 16731 (2008).
26. O. Beckonert *et al.*, *Nat. Protoc.* **2**, 2692 (2007).
27. H. Laue, K. Denger, A. M. Cook, *Appl. Environ. Microbiol.* **63**, 2016 (1997).
28. J. C. Edozien, E. J. Phillips, W. R. F. Collis, *Lancet* **275**, 615 (1960).
29. R. G. Whitehead, R. F. Dean, *Am. J. Clin. Nutr.* **14**, 313 (1964).
30. S. Awwaad, E. A. Eisa, M. El-Essawy, *J. Trop. Med. Hyg.* **65**, 179 (1962).
31. G. Arroyave, D. Wilson, C. DeFunes, M. Béhar, *Am. J. Clin. Nutr.* **11**, 517 (1962).
32. T. R. Ittyerah, S. M. Pereira, M. E. Dumm, *Am. J. Clin. Nutr.* **17**, 11 (1965).
33. T. R. Ittyerah, *Clin. Chim. Acta* **25**, 365 (1969).
34. D. H. Baker, *Prog. Food Nutr. Sci.* **10**, 133 (1986).
35. N. Orentreich, J. R. Matias, A. DeFelice, J. A. Zimmerman, *J. Nutr.* **123**, 269 (1993).
36. M. Mori, S. Manabe, K. Uenishi, S. Sakamoto, *Tokushima J. Exp. Med.* **40**, 35 (1993).
37. J. K. Nicholson, J. A. Timbrell, P. J. Sadler, *Mol. Pharmacol.* **27**, 644 (1985).

Acknowledgments: We thank S. Wagoner, J. Manchester, and M. Meier for superb technical assistance; J. Manchester, S. Deng, and J. Hoisington-López for assistance with DNA sequencing; M. Karlsson, D. O'Donnell, and S. Wagoner for help with gnotobiotic mouse husbandry; W. Van Treuren for writing several scripts, B. Mickelson (Teklad Diets) and H. Sandige for assistance with the design of the mouse diets; and members of the Gordon lab for valuable suggestions during the course of this work. This work was supported by grants from the Bill & Melinda Gates Foundation, and the NIH (DK30292, DK078669, T32-HD049338). M.I.S was the recipient of a postdoctoral fellowship from the St. Louis Children's Discovery Institute (MD112009-201). J.V.L was the recipient of an Imperial College Junior Research Fellowship. Illumina V4-16S rRNA and 454 shotgun pyrosequencing data sets have been deposited with the European Bioinformatics Institute. Specifically, human: V4-16S rRNA data sets (ERP001928) and shotgun sequencing data sets (ERP001911). Mouse: gnotobiotic recipients of discordant twin pair 196: V4-16S rRNA data sets (ERP001861); gnotobiotic recipients of discordant twin pair 196: shotgun sequencing data sets (ERP001819); gnotobiotic recipients of discordant twin pair 57: V4-16S rRNA data sets (ERP001871); gnotobiotic recipients of discordant twin pair 57: shotgun sequencing data sets (ERP001909). Twin pairs were recruited through health centers located in Makhwira, Mitondo, M'biza, Chamba, and Mayaka. Recruitment of participants for the present study, clinical protocols, sample collection procedures, and informed consent documents were all reviewed and approved by the College of Medicine Research Ethics Committee of the University of Malawi and by the Human Research Protection Office of Washington University in St. Louis. All experiments involving mice were performed using protocols approved by the Washington University Animal Studies Committee. Author contributions: M.I.S., T.Y., and J.I.G designed the experiments; M.J.M. designed and implemented the clinical monitoring and sampling for the trial; R.M. and I.T. participated in patient recruitment, sample collection, sample preservation, and clinical evaluations; M.I.S. performed experiments involving gnotobiotic mice, whereas T.Y. characterized microbiota obtained from twins; M.I.S., T.Y., J.C., A.L.K., S.S.R., P.C., J.C.M., J.L., E. Houpt, J.V.L., E. Holmes, and J.N. generated data; M.I.S., T.Y., E. Holmes, J.N., D.K, L.K.U, R.K., and J.I.G. analyzed the results; and M.I.S., T.Y., and J.I.G. wrote the paper.

Supplementary Materials

www.sciencemag.org/cgi/content/full/339/6119/548/DC1
Materials and Methods
Supplementary Text
Figs. S1 to S15
Tables S1 to S10
References (*38*–*54*)

17 August 2012; accepted 10 December 2012
10.1126/science.1229000

REPORTS

A Clock Directly Linking Time to a Particle's Mass

Shau-Yu Lan,[1] Pei-Chen Kuan,[1] Brian Estey,[1] Damon English,[1] Justin M. Brown,[1] Michael A. Hohensee,[1] Holger Müller[1,2]*

Historically, time measurements have been based on oscillation frequencies in systems of particles, from the motion of celestial bodies to atomic transitions. Relativity and quantum mechanics show that even a single particle of mass *m* determines a Compton frequency $\omega_0 = mc^2/\hbar$, where *c* is the speed of light and $\hbar$ is Planck's constant *h* divided by 2π. A clock referenced to ω_0 would enable high-precision mass measurements and a fundamental definition of the second. We demonstrate such a clock using an optical frequency comb to self-reference a Ramsey-Bordé atom interferometer and synchronize an oscillator at a subharmonic of ω_0. This directly demonstrates the connection between time and mass. It allows measurement of microscopic masses with 4×10^{-9} accuracy in the proposed revision to SI units. Together with the Avogadro project, it yields calibrated kilograms.

A particle with mass-energy $E = mc^2$ is represented by a wave oscillating at the Compton frequency $\omega_0 = mc^2/\hbar$ in the particle's rest frame, where *c* is the speed of light and $\hbar$ is Planck's constant *h* divided by 2π (*1*). This is the basis of de Broglie's theory of matter waves (*2*) and underpins modern quantum mechanics and field theory: The time evolution of states is given by wave equations whose plane-wave solutions are proportional to

$$e^{-i\phi} = \exp(-ip_\mu x^\mu/\hbar) = \exp(-i\omega_0\tau) \qquad (1)$$

where $p_\mu = (-m\gamma, m\gamma\boldsymbol{v})$ and x^μ are the momentum and position four-vector, $\tau = t/\gamma$ is the proper time, γ is the Lorentz factor, and $\boldsymbol{v}$ and *t* are the laboratory-frame velocity and time. Much has been theorized about the physical reality of quantum states as "oscillators" (*3*–*7*), but surprisingly few experiments have been proposed to address this topic (*8*). Here, we directly address a consequence of Eq. 1 that has deep physical and perhaps even cosmological implications: Because the oscillations of a wave packet accumulate phase $\omega_0\tau$ just like a clock following the same

[1]Department of Physics, 366 Le Conte Hall MS7300, University of California, Berkeley, CA 94720, USA. [2]Lawrence Berkeley National Laboratory, One Cyclotron Road, Berkeley, CA 94720, USA.

*To whom correspondence should be addressed. E-mail: hm@berkeley.edu

trajectory, it has been suggested that the passage of time is observable as soon as the universe contains massive particles (*1*). It ought to be possible to build a Compton clock: a clock referenced to the mass of a single particle.

Advances in timekeeping (*9*–*12*) have followed the use of references with higher frequency, increased quality factor Q, and lowered instability from systematic influences. The Compton frequency of a stable particle is high ($\omega_0/2\pi = 3 \times 10^{25}$ Hz for a cesium atom), has virtually infinite quality factor $Q = \omega_0/\Gamma$, where $1/\Gamma$ is the particle's $1/e$ lifetime, and is one of the most stable quantities in nature. In principle, a Compton-frequency clock could be built by annihilating a particle-antiparticle pair and counting the frequencies of the generated photons. However, this frequency is far beyond modern counting techniques; to access it, we require a method of dividing it into a technically accessible range.

Here, we present a Compton clock by combining an atom interferometer with an optical frequency comb. In a Ramsey-Bordé atom interferometer (Fig. 1) (*7*, *13*), a quantum wave packet initially at rest interacts with a pulse of two counterpropagating laser beams having laboratory-frame frequencies of $\omega_\pm$ and wavenumbers of $k_\pm$, respectively. The wave packet absorbs n photons from the first beam while being stimulated to emit n photons into the second beam, without modifying its internal state through multiphoton Bragg diffraction (*14*, *15*). By appropriate choice of the laser intensity and pulse duration, the process occurs with a probability of 50%, splitting the wave packet. While the first partial wave packet remains at rest, the second moves away with a laboratory-frame momentum $p = n\hbar(k_+ + k_-)$. It is convenient to introduce a rapidity parameter ρ so that $p = mc\sinh(\rho)$ and the Lorentz factor $\gamma = [1 - v^2/c^2]^{-1/2} = \cosh(\rho)$. Energy-momentum conservation (the Bragg condition) provides the relation

$$\omega_\pm = \omega_L e^{\pm\rho/2} \qquad (2)$$

where $\omega_L = \omega_0\sinh(\rho/2)/n$. [In the nonrelativistic limit, $\omega_L \approx (\omega_+ + \omega_-)/2 \equiv kc$ and $\omega_\pm \approx \omega_L(1 \pm n\hbar k/mc)$.] Interaction with four laser pulses (Fig. 1) brings the wave packets together for interference.

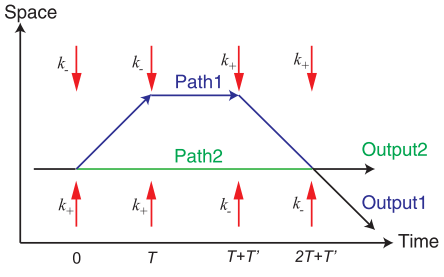

Fig. 1. Paths of the matter waves in a Ramsey-Bordé interferometer versus time; red arrows denote laser beams. Additional paths that do not interfere are not shown. The diagram is drawn in a freely falling inertial frame, and does not show the free fall of the atoms.

The probability of detecting the particle at the outputs (Fig. 1) is given by $\cos^2(\Delta\varphi/2)$, where $\Delta\varphi$ is the relative phase of the wave packets. In a relativistic, semiclassical treatment, Eq. 1 shows that the wave packets acquire a relative phase of $\Delta\varphi_{free} = \omega_0[\tau^{(1)} - \tau^{(2)}] = 2\omega_0 T(\gamma^{-1} - 1)$ (nonrelativistically, $\Delta\varphi_{free} \approx -4n^2\hbar k^2 T/m$) during their free evolution between the laser pulses (*3*), where $\tau^{(1,2)}$ are the proper times on paths 1 and 2. Their difference $\tau^{(1)} - \tau^{(2)}$ is related to the laboratory-frame time by a factor $\gamma^{-1} - 1$, which is determined by the laser frequencies by Eq. 2 and can be used to divide the Compton frequency into a technically accessible range. Synchronizing an oscillator to the divided Compton frequency is accomplished as follows: In the experiment, this oscillator sets the frequency difference $\omega_m \equiv \omega_+ - \omega_-$ between the counterpropagating laser beams. Whenever the particle absorbs a photon, the phase of the photon is added to the wave packet's phase and subtracted for stimulated emission. It can be shown (*16*) that the sum $\Delta\varphi_{laser}$ of these phases (eq. S2) cancels the free evolution phase $\Delta\varphi_{free}$ exactly if, and only if, $\omega_\pm$ satisfy Eq. 2, so that

$$\omega_m = \frac{2n\omega_L^2}{\omega_0} \qquad (3)$$

The phase cancellation $\Delta\varphi = \Delta\varphi_{laser} + \Delta\varphi_{free} = 0$ is verified by observing the interference fringes of the particle at the interferometer output and maintained by feedback to the oscillator.

Ramsey-Bordé interferometers are routinely used to measure $\hbar/m$ (*17*), but such measurements of $\hbar/m$ are not themselves clocks because they are reliant upon an external frequency reference to measure ω_L. We use an optical frequency comb to set $\omega_L = N\omega_m$, eliminating the laser frequency as a free parameter. Combined with Eq. 3, we obtain

$$\omega_m = \frac{\omega_0}{(2nN^2)} \qquad (4)$$

which is an exact result in this relativistic and semiclassical picture, showing that ω_m is determined solely by the Compton frequency. Corrections from nonclassical paths are negligible here. We are free to choose any value for n and N and lock the oscillator directly to the Compton frequency or a subharmonic without changing the underlying physics. For example, $n = 2$ and $N = 1/2$ yields $\omega_0 = \omega_m = 2\omega_L$ and $\omega_\pm = \omega_L(1 + \sqrt{2})^{\pm 1}$. In practice, N is chosen so that ω_L and ω_m are accessible to existing technologies. The experiment is a Compton clock by virtue of the fact that it self-references the laser frequency through the optical frequency comb, which ensures that the output frequency ω_m is fully determined by the Compton frequency and known ratios. It is independent of any external standards. The self-referenced atom interferometer serves as a clockwork that links the frequency of our master oscillator to the Compton frequency of the matter wave packets.

Our experiment uses cesium-133 atoms because they are amenable to the techniques of atom optics and are electrically neutral, which reduces systematic effects. Because their internal structure is not relevant to ω_m, the atoms approximate noninteracting point masses. Our atom interferometer has been described in detail elsewhere (*15*). The clock's operation is illustrated in Fig. 2. A voltage-controlled 10-MHz crystal oscillator O1 [FTS 1050A (Symmetricom, Beverly, MA)] with frequency ω_{cryst} is the master oscillator for all

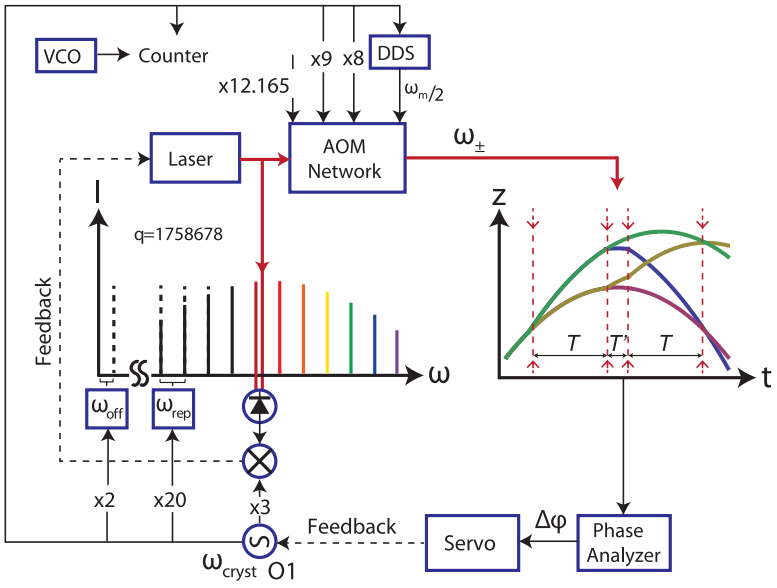

Fig. 2. Schematic. Oscillator O1 is the frequency reference for all signal generators and the optical frequency comb. The laser used to address the atom interferometer is phase-locked to the comb. Shown in the diagram is the freely falling atomic trajectories versus time for the simultaneous conjugate interferometers (the lower of which being shown in Fig. 1) used to cancel the gravity-induced phase. The phase measurement from the atom interferometer provides an error signal to O1 in order to close the feedback loop.

frequency sources, pulse generators, and lasers involved in the experiment. The frequency comb stabilizes the laser frequency to $N_c\omega_{cryst}$, where N_c = 35,173,594.165 (*16*). A direct digital synthesizer (DDS) generates $\omega_m/2 = N_{DDS}\omega_{cryst}$ at ~82 kHz, and acousto-optical modulators (AOMs) generate $\omega_\pm$ by applying the relation $\omega_\pm = \omega_L \pm \omega_m/2$ (valid in the nonrelativistic limit), where N_{DDS} = 2,326,621,801,616/2^{48}. The factor N is thus $N = N_c/N_{DDS}$ = 4,255,305,521.31286. Another AOM shapes the time domain profile of the laser pulses. Our signal to noise is optimal for 5th-order Bragg diffraction (n = 5) with a pulse separation time (Fig. 1) T = 160 ms. The atomic population at the interferometer output is determined by means of fluorescence detection and then processed to yield the interferometer phase $\Delta\varphi = \Delta\varphi_{laser} + \Delta\varphi_{free}$.

A feedback loop adjusts ω_{cryst} so as to maintain $\Delta\varphi = 0$. Its operation is demonstrated in Fig. 3: The first 10 data points are taken during normal operation. At the 11th data point, we briefly disable the feedback, so that ω_{cryst} is free-running, and the experiment performs a Ramsey-Bordé photon recoil measurement. The measured signal is then proportional to $\omega_L^2 = (N_c\omega_{cryst})^2$ (Eq. 3). Increasing N_c by 100 parts per billion (ppb) increases ω_L and produces a 200-ppb increase in $\Delta\varphi_{free}$ (Fig. 3, shaded area). At the 13th data point, the feedback is restored. Because the feedback stabilizes ω_{cryst} to a value inversely proportional to N_c^2 (Eq. 4), the signal frequency decreases by 400 ppb, equilibrating 200 ppb lower than the first 10 data points (Fig. 3), which is opposite to the observed shift for a recoil measurement.

Quantitative agreement is demonstrated by comparing the rest-mass stabilized frequency ω_{cryst} with a rubidium frequency standard [SRS FS725 (Stanford Research Systems, Sunnyvale, CA)] over 6 hours (Fig. 4A). It averages to 9,999,998.127 Hz with a SD of the mean of 0.015 Hz. A χ^2 test (Fig. 4B) yields a normalized χ^2 = 1.4. Our statistical uncertainty is 0.015 Hz × $(\chi^2)^{1/2}$ = 0.018 Hz, or 1.8 ppb. Using Eq. 4 and correcting for systematic effects (*16*), we obtain the Compton frequency $\omega_0/2\pi$ = (2,993,486,252 ± 12) × 10^{16} Hz. The deviation from the expected values (*16*, *18*) is –5.2 ± 4.0 ppb and is consistent with zero within 2σ. The Allan variance (Fig. 4C) is below $10^{-8}/[\tau/(1000\ s)]^{1/2}$, where τ is the integration time.

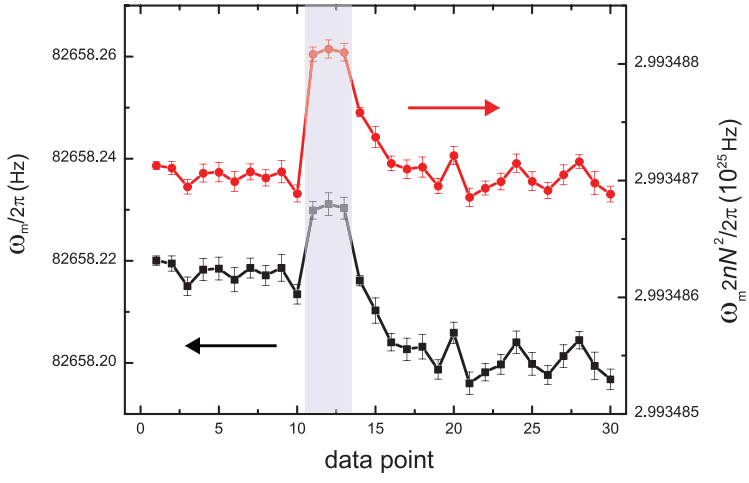

Fig. 3. Measured frequency ω_m (lower trace; left axis) as well as $\omega_m(2nN^2)$ (upper trace; right axis) shows the action of the feedback loop. During the shaded interval, the feedback is disabled.

Although this accuracy is modest, similar to the first cesium atomic clocks (*9*), the resolution and accuracy of atom interferometry is advancing rapidly (*19*). Up to 100-fold improvement in resolution could be obtained by approaching the shot noise limit of our interferometer. Use of higher laser frequencies (which is possible without changing the reference particle), lighter particles, and/or longer interrogation times can possibly lead to a Compton clock that can serve as a primary time standard. The intrinsic stability and Q factor of a stable particle's Compton frequency is unmatched by any other frequency reference. Mass, frequency, time, and length could all be derived from one fundamental unit, defined by a specific particle.

The clock can also be used for the opposite purpose, measuring mass by measuring the Compton frequency. In 2011, the General Conference on Weights and Measures (CGPM-2011) considered a revision to the SI units that would assign an exact value to the Planck constant h (*20*). The kilogram would then be referenced to the second through the defined values of the Planck constant and the speed of light. Microscopic masses could be related to the fine structure constant (*21*, *22*) or h/M (*17*); macroscopic masses could be measured by using the Watt balance (*23*, *24*). These methods, however, require auxiliary measurements and/or intricate theory (*16*). The Compton clock would provide an absolute measurement of the cesium atom's mass to an accuracy of 4.0 ppb, which is competitive with other methods and greater than 10 times more accurate than in the present SI (*18*). Other microscopic masses can be related to the cesium mass by means of mass spectroscopy.

The link to macroscopic masses can be made by Avogadro spheres: silicon crystals of accurately measured volume V and lattice constant a (*25*). In theory, the number of atoms contained in such a crystal is $N_{at} = 8V/a^3$, where 8 is the number of atoms in the unit cell. Because binding energies are negligible, the Compton frequency of the sphere is $\omega_M = [m(\mathrm{Si})/m(^{133}\mathrm{Cs})]N_{at}\,\omega_{Cs}$, given by the measured Compton frequency of

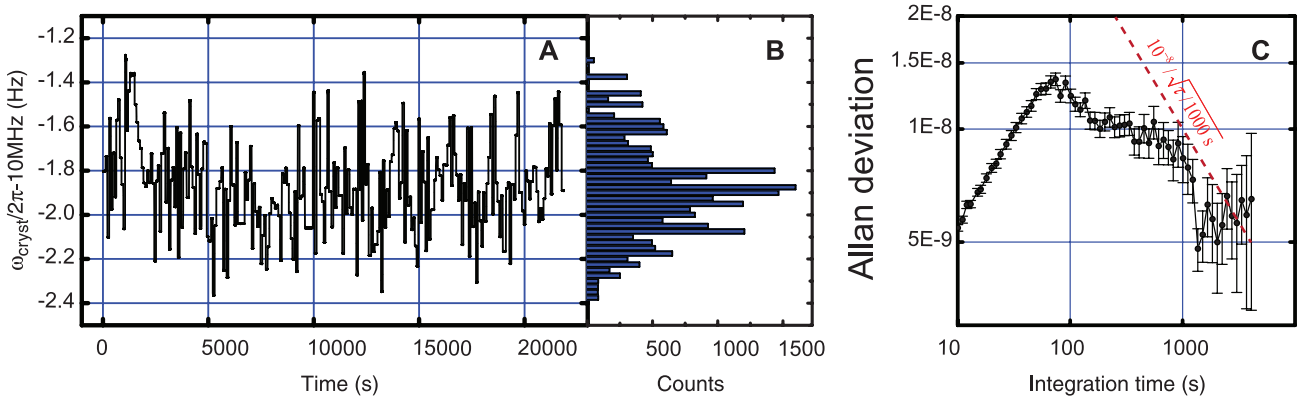

Fig. 4. Compton clock performance. (**A**) Frequency minus 10 MHz versus time plotted over ~6 hours. (**B**) Histogram of data (bin size = 0.025 Hz). (**C**) Root Allan variance (RAV) of the data in (A). It is $<10^{-8}/(\tau/1000\ s)^{1/2}$ between integration times τ of ~100 s and ~ 1 hour. The slope between τ = 10 and 100 s is an artifact of the 80-s update cycle of the experiment.

cesium atoms ω_{Cs}. This yields its mass as $M = \omega_M \hbar / c^2$. The ratio $m(\mathrm{Si})/m(^{133}\mathrm{Cs})$ is between the effective molar mass of the sphere's material and cesium-133. According to (*25*), present data yields the spheres' mass with an overall accuracy of 30 ppb so that they would constitute the most accurately calibrated macroscopic masses under the proposed CGPM-2011 redefinition—a testament to the precision achieved in constructing Avogadro spheres.

Although any method for measuring microscopic mass can be used, the Compton clock offers a transparent connection between the second and a microscopic mass on the basis of simple physical principles without requiring auxiliary measurements. It directly realizes a long-standing proposal to measure mass in terms of the Compton frequency (*6*). The method outlined here offers a different set of systematic effects as compared with Watt balances (*23*, *24*), thus serving as an important test of the overall consistency of the laws of physics and experimental methods. It is based on a body's inertial rather than gravitational mass. In the context of the present SI, the combination of the Avogadro project and the Compton clock serves as a measurement of the Planck constant.

Looking forward, the rapidly developing field of optomechanics (*26*) might enable measurements of the single-photon recoil energy of a nanomechanical mirror. This could result in a clock referenced to the mass of a mesoscopic object, or a mesoscopic mass standard. Because Bragg diffraction of electrons has already been demonstrated (*27*), a clock using elementary particles or even antiparticles is possible. Such clocks would be useful for testing CPT symmetry or the Einstein Equivalence Principle for antimatter.

We have demonstrated a clock stabilized to the rest mass of a particle. It highlights the intimate connection between frequency and mass. It proves that massive particles can serve as a frequency reference without requiring their mass to be converted to energy as an explicit illustration of a key principle of quantum mechanics. Furthermore, we have shown that a single massive particle is sufficient to measure time.

References and Notes

1. R. Penrose, *Cycles of Time: An Extraordinary View of The Universe* (Knopf, New York, 2011), sec. 2.3.
2. L. De Broglie, thesis, University of Paris, Paris, France (1924).
3. H. Müller, A. Peters, S. Chu, *Nature* **463**, 926 (2010).
4. M. A. Hohensee, S. Chu, A. Peters, H. Müller, *Phys. Rev. Lett.* **106**, 151102 (2011).
5. P. Wolf *et al.*, *Class. Quantum Gravity* **28**, 145017 (2011).
6. J. W. G. Wignall, *Phys. Rev. Lett.* **68**, 5 (1992).
7. Ch. J. Bordé, *Eur. Phys. J. Spec. Top.* **163**, 315 (2008).
8. M. A. Hohensee, B. Estey, P. Hamilton, A. Zeilinger, H. Müller, *Phys. Rev. Lett.* **108**, 230404 (2012).
9. L. Essen, J. V. L. Parry, *Nature* **176**, 280 (1955).
10. T. E. Parker, *Metrologia* **47**, 1 (2010).
11. A. D. Ludlow *et al.*, *Science* **319**, 1805 (2008).
12. C. W. Chou, D. B. Hume, J. C. J. Koelemeij, D. J. Wineland, T. Rosenband, *Phys. Rev. Lett.* **104**, 070802 (2010).
13. A. D. Cronin, J. Schmiedmayer, D. E. Pritchard, *Rev. Mod. Phys.* **81**, 1051 (2009).
14. H. Müller, S.-W. Chiow, Q. Long, S. Herrmann, S. Chu, *Phys. Rev. Lett.* **100**, 180405 (2008).
15. S.-Y. Lan, P.-C. Kuan, B. Estey, P. Haslinger, H. Müller, *Phys. Rev. Lett.* **108**, 090402 (2012).
16. Materials and methods are available as supplementary materials on *Science* Online.
17. R. Bouchendira, P. Cladé, S. Guellati-Khélifa, F. Nez, F. Biraben, *Phys. Rev. Lett.* **106**, 080801 (2011).
18. P. J. Mohr, B. N. Taylor, D. B. Newell, *The 2010 CODATA Recommended Values of the Fundamental Physical Constants* (Web Version 6.0); http://physics.nist.gov/constants.
19. S. Dimopoulos, P. W. Graham, J. M. Hogan, M. A. Kasevich, *Phys. Rev. Lett.* **98**, 111102 (2007).
20. "Resolution 1: On the possible future revision of the International System of Units, the SI," General Conference on Weights and Measures, Sèvres, France, 17 to 21 October 2011.
21. D. Hanneke, S. Fogwell, G. Gabrielse, *Phys. Rev. Lett.* **100**, 120801 (2008).
22. T. Aoyama, M. Hayakawa, T. Kinoshita, M. Nio, *Phys. Rev. Lett.* **109**, 111807 (2012).
23. I. A. Robinson, B. P. Kibble, *Metrologia* **44**, 427 (2007).
24. R. L. Steiner, E. R. Williams, R. Liu, D. B. Newell, *IEEE Trans. Instrum. Meas.* **56**, 592 (2007).
25. B. Andreas *et al.*, *Phys. Rev. Lett.* **106**, 030801 (2011).
26. T. J. Kippenberg, K. J. Vahala, *Science* **321**, 1172 (2008).
27. D. L. Freimund, H. Batelaan, *Phys. Rev. Lett.* **89**, 283602 (2002).

Acknowledgments: We thank S. Chu, P. Hamilton, and M. Kasevich for stimulating discussions; D. Budker, P. Kehaiyas, G. Kim, M. Xu, E. Ronayne Sohr, and D. Schlippert for experimental assistance; and A. Brachmann, R. Falcone, and W. E. White for providing a laser. J.M.B. acknowledges support by the Miller Institute for Basic Research in Science. This work was supported by the Alfred P. Sloan Foundation, the David and Lucile Packard Foundation, the National Institute of Standards and Technology, the National Science Foundation, and the National Aeronautics and Space Administration.

Supplementary Materials

www.sciencemag.org/cgi/content/full/science.1230767/DC1
Materials and Methods
Supplementary Text
Figs. S1 and S2
Table S1
References (*28*–*32*)

26 September 2012; accepted 20 November 2012
Published online 10 January 2013;
10.1126/science.1230767

Nanoscale Nuclear Magnetic Resonance with a Nitrogen-Vacancy Spin Sensor

H. J. Mamin,[1] M. Kim,[1,2] M. H. Sherwood,[1] C. T. Rettner,[1] K. Ohno,[3] D. D. Awschalom,[3] D. Rugar[1]*

Extension of nuclear magnetic resonance (NMR) to nanoscale samples has been a longstanding challenge because of the insensitivity of conventional detection methods. We demonstrated the use of an individual, near-surface nitrogen-vacancy (NV) center in diamond as a sensor to detect proton NMR in an organic sample located external to the diamond. Using a combination of electron spin echoes and proton spin manipulation, we showed that the NV center senses the nanotesla field fluctuations from the protons, enabling both time-domain and spectroscopic NMR measurements on the nanometer scale.

Both nuclear magnetic resonance (NMR) spectroscopy and magnetic resonance imaging (MRI) have become indispensable tools in many diverse fields of research, including analytical chemistry, materials science, structural biology, neuroscience, and medicine (*1*). The one major deficiency of NMR is the low sensitivity of the conventional coil-based induction method of detection, which prevents its application to samples at the nanometer scale (*2*). Much improved detection sensitivity has been achieved with magnetic resonance force microscopy, which is based on detecting weak magnetic forces in the presence of a strong field gradient and has demonstrated nanometer-scale NMR imaging at cryogenic temperatures (*3*). Here, we present an alternative nanoscale detection method that works in the absence of a magnetic field gradient, thus preserving spectroscopic information, and is operable over a wide range of temperatures, including room temperature. A single near-surface nitrogen-vacancy (NV) center in diamond is used as an atomic-size sensor to detect weak magnetic fields originating from nuclear spins external to the diamond. In an initial demonstration, we detected randomly polarized hydrogen nuclei (protons) in an organic polymer. Both time domain and spectroscopic information were obtained by appropriately manipulating the protons so as to affect the precession phase of the highly coherent NV electron spin. The results suggest that NV-based NMR detection may provide a path toward three-dimensional nanoscale magnetic resonance imaging (nanoMRI) under ambient conditions (*4*, *5*).

NV centers are proving to be particularly useful for both quantum information processing and nanoscale magnetic sensing (*6*–*11*). The negatively charged center has a spin state with a long coherence time, especially in isotopically purified crystals (*12*, *13*), and an electronic-level structure

[1]IBM Research Division, Almaden Research Center, San Jose, CA 95120, USA. [2]Center for Probing the Nanoscale, Stanford University, Stanford, CA 94305, USA. [3]Center for Spintronics and Quantum Computation, University of California, Santa Barbara, CA 93106, USA.

*To whom correspondence should be addressed. E-mail: rugar@us.ibm.com